Experiments in Fluids (2025) 66:130
https://doi.org/10.1007/s00348-025-04032-x

RESEARCH ARTICLE

Effect of throat diameter on the cavitation phenomenon inside an aerated Venturi tube for microbubble production

Noor Saffreena Hamdan[1,3] · Akiko Kaneko[2]

Received: 10 July 2024 / Revised: 25 March 2025 / Accepted: 8 April 2025

Abstract
Aeration in Venturi tubes for microbubbles production has become popular in recent years as it enhanced the transportation of oxygen and other gases in wastewater treatment and mineral engineering. In an aerated Venturi, air/gas was injected upstream into the flowing liquid inside the Venturi tube. The air flows inside the Venturi tube as bubbles, before breakup occurs downstream after the throat area. This method promoted the transportation of particular gases or substances in microbubbles. To further increase the generation of microbubbles, flowing liquid velocity was increased by decreasing the throat diameter, but cavitation started to emerge inside the tube as velocity increased. This present study aims to investigate the effect of reducing the throat diameter on the cavitation number of the aerated Venturi tube and how it affects the breakup characteristics of bubbles. Activities involved in the investigation were: visualization of flow and generated microbubbles, image processing of the images captured, pressure and void fraction measurement, and calculating the cavitation number. The result showed that reducing the throat diameter initiated the cavitation occurrence earlier, and in aerated cases, cavitation exists in the form of cavitated bubbles. Aeration also affects the cavitation number in a non-cavitated flow but does not significantly affect the existing cavitated flow. Reducing the throat diameter also successfully increased the generation of bubbles less than 0.2 mm, but the overall SMD did not show a straightforward relationship with cavitation number.

1 Introduction

Over the decades, researchers have focused on microbubbles for their amazing abilities in various industries. They were usually produced by the microbubble generator. Among the different types, the Venturi-type microbubble generator captured the attention due to its simple mechanism, simple design, and low-cost features. Utilizing the Venturi tube, microbubbles were generated as the liquid flowed through the convergence area and the sudden change in tube size reduced the local pressure. As the flowing liquid increased in velocity, the pressure dropped further, and cavitated bubbles started to emerge to produce microbubbles (Brennen 2002). Generally, the generated microbubbles have diameters less than 200 µm with great surface tension that promoted them to exist longer in liquid. Due to their special characteristics, microbubbles were employed as a transporter in agricultural and medical sciences. They were also utilized as an imaging contrast agent to improve the assessment in imaging exams. In wastewater treatment, microbubbles had a high potential for the dissolution of oxygen, fragmentation of organic particles, floatation of minerals, and suppression of microalgae growth (Terasaka et al. 2011; Wen et al. 2011; Li et al. 2019). For these purposes, air or gas was introduced to the flowing liquid, and aeration was executed. Aeration was expected to increase the generated microbubbles count and reduce cavitation's corrosion effects. This aeration method is shown in Fig. 1. Air was injected before the throat, and microbubbles were generated at the diverging part. The microbubble generation mechanism at the diverging part depended on the flow velocity.

In one related research, the bubble collapsed behavior in aeration conditions was explained using a single bubble, and breakup behavior was reported to be linked with pressure recovery (Fujiwara et al. 2007). This was further clarified by

✉ Noor Saffreena Hamdan
saffreena@utem.edu.my

✉ Akiko Kaneko
kaneko@kz.tsukuba.ac.jp

[1] Graduate School of Systems and Information Engineering, University of Tsukuba, Tsukuba, Japan

[2] Institute of Systems and Information Engineering, University of Tsukuba, Tsukuba, Japan

[3] Fakulti Teknologi dan Kejuruteraan Mekanikal, Universiti Teknikal Malaysia Melaka, Melaka, Malaysia

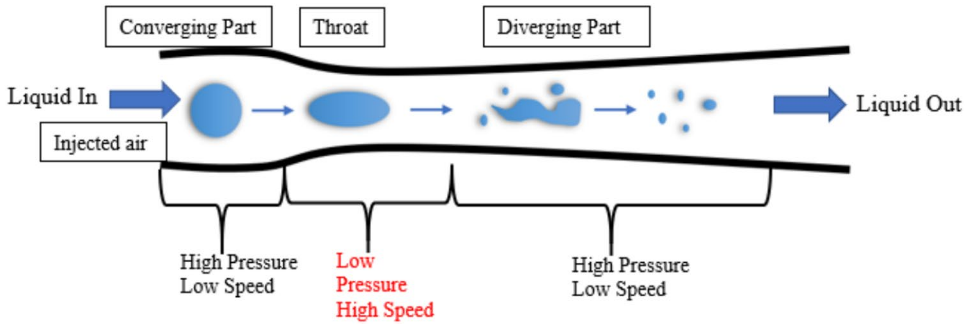

Fig. 1 Aeration method using Venturi tube

a recent study, which claimed that the collapse of bubbles owing to pressure variation was caused by the initial bubble size that was substantially greater than the Kolmogorov scale (Ni 2024). Another researcher executed detailed experiments with the aeration method under different air flow rates. The void fraction and pressure measurement revealed that changes in the flow velocity occurred between the throat and the bubble breakup point. Thus, the Mach number of the flow was determined further to investigate the velocity characteristics toward the speed of sound. Shockwave existence was also suggested when the velocity exceeded the speed of sound (Fujii et al. 2018). In many other studies, the air was sucked at the throat area. Although this method was slightly different, it was sufficient as a reference for the current study. Through the suction of air from the throat area, it was found that increasing the diverging angle moderately and decreasing the throat size improved the performance of the Venturi microbubble generator (Huang et al. 2021, 2019; Liu et al. 2020). It is also well established from various studies that although increasing the flowing liquid velocity decreases the generated bubble sizes, increasing the air flow rate has the opposite effect (Gordiychuk et al. 2016; Zhao et al. 2017; Sun et al. 2017).

Nevertheless, most of these studies considered bubbles with a diameter of more than 0.2 mm in their result as visualization of bubbles less than 0.2 mm requires advanced visualization techniques. On the other hand, most of these studies did not discuss the cavitation phenomenon that existed as the flowing liquid velocity increased to produce more microbubbles in the aeration method.

Much uncertainty about cavitation in conditions where aeration exists alongside a flowing liquid in the Venturi tube is still unknown. To study this, Tomov et al. (2016) aerated three different cavitation regimes in a flowing liquid inside a Venturi tube, attempting to influence the cavitation inception of a cavitating liquid. They found out that the tendency of the injected air bubbles to break up into smaller bubbles depends on the type of the initial cavitation condition of the liquid. However, this study did not relate the findings with generated microbubbles (Tomov et al. 2016). In another study, Kido executed an experiment where aeration was done from the beginning, using a 6-mm Venturi tube, and revealed the cavitation number of this multiphase flow (Kido et al. 2021). The cavitation number was then compared in a study by Saffrena with a 4-mm Venturi tube, and the bubble breakup characteristics were discussed briefly (Saffreena and Kaneko 2022). Nonetheless, in both articles, the changes in cavitation phenomena and the breakup process, when the throat diameter was reduced, were not discussed in detail. The distribution of microbubbles less than 0.2 mm when reducing the throat diameter and its relation to cavitation number were also not investigated.

Therefore, the objective of our study was to investigate the changes in cavitation number in aerated Venturi tubes as we reduce the throat diameter. We also evaluated the effects of the cavitation number on the generated microbubbles, especially for bubbles with diameters less than 0.2 mm. Two different throat sizes of Venturi tubes were utilized, while other geometric parameters of the tube were maintained to reduce the effect of other variables. The investigation includes visualization, pressure and void fraction measurement along the tube, and calculation of cavitation number for both different throat sizes. Finally, the microbubbles produced were evaluated, giving focus to bubbles with less than 0.2 mm in diameter, to establish a connection between the results and the role of the Venturi tube as a microbubble generator.

2 Method

2.1 Experimental apparatus

Figure 2 depicts an experimental setup for creating an aerated flow inside a Venturi tube. The setup included a 200-L tank with an internal baffle, a centrifugal pump, a liquid flow meter, an airflow meter, a compressor to deliver air, and a Venturi tube. In the experiment, tap water, filtered through 5-µm mesh, was pumped from the tank, through the Venturi tube, and then circulated back to the tank. Experiments were done at room temperature under atmospheric pressure. For the aeration purpose, the air was supplied below the

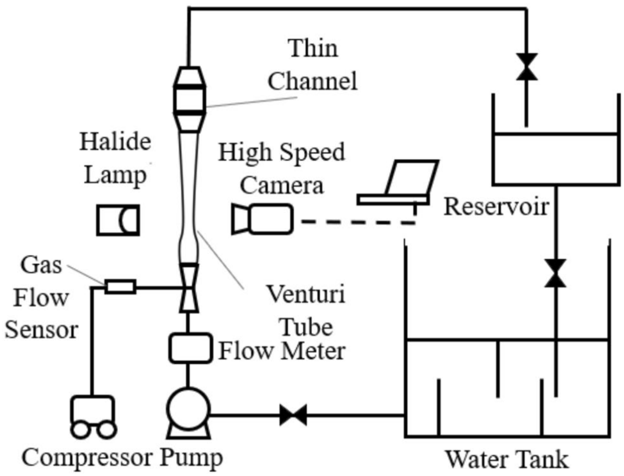

Fig. 2 Experimental setup

Venturi tube with the flow rate adjusted using an airflow sensor (KEYENCE FD-V40 series). A thin channel with a 3-mm slit width was located on top of the Venturi tube location in the apparatus to allow the distributed flow of bubbles to form at the outlet. Acrylic was used as the material for better visualization of the distributed bubbles.

The geometric dimensions of the two Venturi tubes used in this experiment are illustrated in Fig. 3. The tubes were fabricated from acrylic and were 150 mm in length, with an inlet and outlet diameter of 16 mm and 2 mm throat length. The length was made to be long enough to allow the collapse of bubbles from the breakup region into smaller bubbles. The diverging angle was manufactured to be 6° to reduce the occurrence of boundary layer separation. It has been established that an angle of about 6–7°contributes to the optimum balance between length and the probability of boundary layer separation, thus reducing energy losses

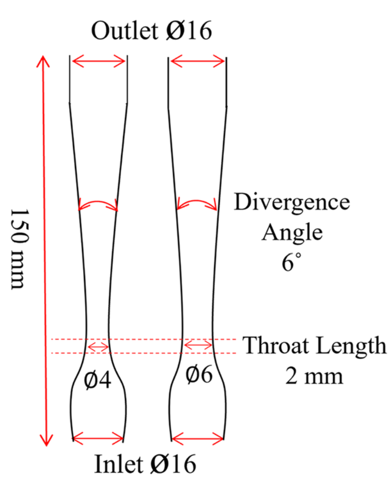

Fig. 3 Geometric dimension of venturi tube used in the experiment

(Bashir et al. 2011). These parameters were identical for both tubes to minimize the effect of other variables on the results. However, the throat diameters were fabricated to be 4, and 6 mm each to observe the effect of decreasing throat diameter on the result. The tubes will be indicated as $d_{th}=4$ and 6 mm from now on.

2.2 Experimental conditions

The working fluid in this study was assumed as an incompressible flow, and the velocity was represented by the superficial velocity. Superficial velocity was defined as the volumetric flow rate of the fluid divided by the cross-sectional area it flows through as shown in Eq. (1). The supplied air in this study was presented by airflow ratio, as shown in Eq. (2). Both flow rate for water and air was adjusted using a liquid flow meter and an airflow sensor. The ranges of these two parameters are concluded in Table 1. As it was hard to compare each tube condition as the inlet pressure was not set and Reynolds numbers were not appropriate to resemble a multiphase flow, the condition for both different throat sizes tubes was compiled under the superficial throat velocity and was indicated as j_{th}. Equation (1) was used to define j_{th} with A as the cross-sectional area of the $d_{th}=4$ mm and 6 mm, respectively. We agreed that this superficial velocity was more accurate than the throat velocity determined by Bernoulli's equation for multiphase flow conditions.

The range was selected by referring to the homogenous flow model of the two-phase flow presented in Fig. 4, under the presumption that the working liquid was isothermal and homogenous (Wijngaarden 1972). The dashed line depicted the condition of flow for each tube when the superficial velocity at the throat was equal to the speed of sound under

Table 1 Experimental conditions range

Superficial throat velocity, j_{th} [m/s]	Superficial liquid inlet velocity, j_{Lin} [m/s]		Airflow ratio, β[-]
	$d_{th}=4$ mm	$d_{th}=6$ mm	
10	06	1.5	0.016
			0.035
			0.063
15	1.1	2.1	0.016
			0.035
			0.063
20	1.3	2.5	0.016
			0.035
			0.063
25	1.6	3.5	0.016
			0.035
			0.063

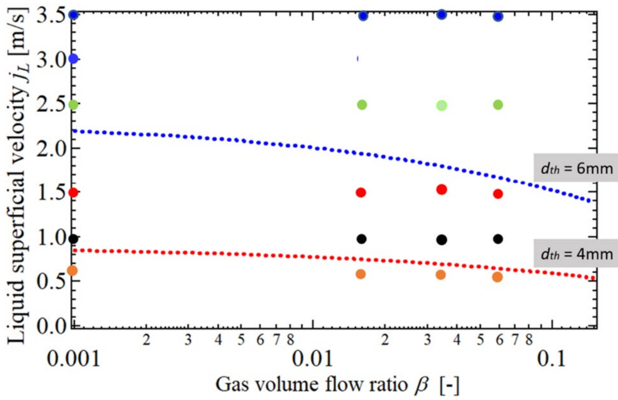

Fig. 4 Homogenous flow model of two-phase flow

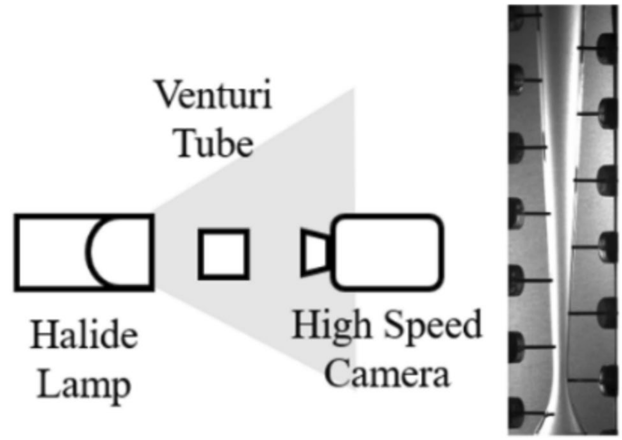

Fig. 5 Shadowgraphy method and example of flow visualization

the presumed condition. The condition above each dashed line represents a supersonic flow condition, while the condition below the dashed line represents a subsonic flow condition. The blue line represents 6-mm Venturi tube, while the red line represents the 4-mm Venturi tube. Two flow conditions above the dashed line and two flow conditions below the dashed line were chosen for each tube, as the experiment condition.

$$j = \frac{Q_L}{A} \tag{1}$$

$$\beta = \frac{Q_G}{Q_G + Q_L} \tag{2}$$

2.3 Visualization

In this experiment, the visualization was performed through the shadowgraphy method. The shadowgraphy method and example of visualization are presented in Fig. 5. Shadowgraphy was a method where the targeted object was placed in the middle of a high-speed camera and a light source. The targeted object blocks the light from the light source, resulting in a dark spot in the camera images. As the Venturi tube was made from acrylic, the inner curved surface of the tube did not cause image distortion due to refraction as acrylic has a relatively close refractive index to water.

The visualization was performed in two parts using a Photron Mini AX-200 high-speed camera with LAOWA 100 mmF/2.8 2 × Ultra Macro with 400 frame rate per second, lens system. Red LED and metal halide lamps were utilized depending on the brightness required for each visualization activity. The frame rate and shutter speed were adjusted for different visualizations to get the best result.

The first part of the visualization was along the Venturi tube where the bubble breakup dynamic was captured. Halogen lamps act as a light source as brightness is crucial, especially in a high-flow-ratio condition. The second part was after the outlet where generated microbubbles dispersed through a thin channel with a slit of 3 mm. In this part, the area for visualization is set to be 4 × 4 pixels, and image resolution with accuracy up to 1 pixel = 9.6±0.5 µm was achieved using the LAOWA 2 × Ultra Macro lens with the lower limit of 2 pixels. The image captured was processed using the Python programming language through the Python Imaging Library (PIL). Background subtraction and image binarization were done before the captured bubble area was calculated as the contour area as shown in Fig. 6. The generated bubble size was retrieved and the Sauter mean diameter of the bubbles was calculated. The frame rate per second (FPS) was set to be 5000 FPS for flow visualization and 7200 for bubble visualization with exposure time varied between 0.33 and 5 µS.

2.4 Pressure and voltage measurement

An approach based on the procedure of Uesawa et al. (2012) was adopted to acquire a better understanding of cavitation in an aerated Venturi tube, where pressure and voltage were recorded at specific places along the tube using the apparatus illustrated in Fig. 7(a) and (b) (Uesawa et al. 2012). Each location of a flow valve or a compression fitting was distanced 10 mm from each other. The throat was taken as $z = 0$ mm. To carry out the pressure measurement, the flow valve was connected to a transducer via a tube, and the data were recorded using a data logger with a 5-kHz sampling frequency in 5 s. In this measurement, zero references were made against the atmospheric pressure.

As for the voltage measurement, a DC constant-current source supplied current to the flowing liquid through two

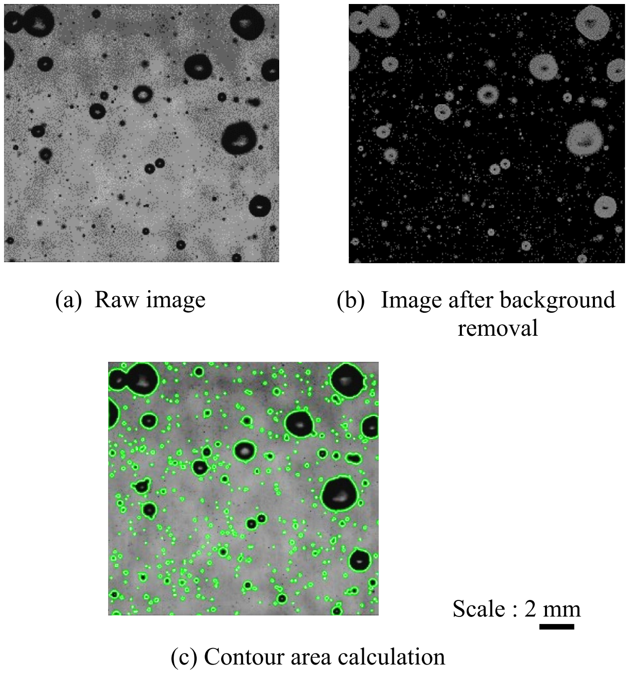

Fig. 6 Example of image processing steps to determine bubble sizes

stainless steel electrode rings positioned at the inlet and outlet of the Venturi tube. Then, two voltage-measuring probes were clipped at two selected compression fittings opposite to each other, allowing measurement of the voltage between the two points of the set region. The measurement time range was 0.5 s with a sampling frequency of 100 kHz. The error of this measurement system was about ± 9% of the measurement value with 91% accuracy. Later, the void fraction was then estimated using Eq. (3). In this equation, v' is the voltage ratio of the gas–liquid flow, normalized by single-phase liquid flow.

$$\left(\alpha = \frac{v' - 1}{v' + 0.5}\right) \tag{3}$$

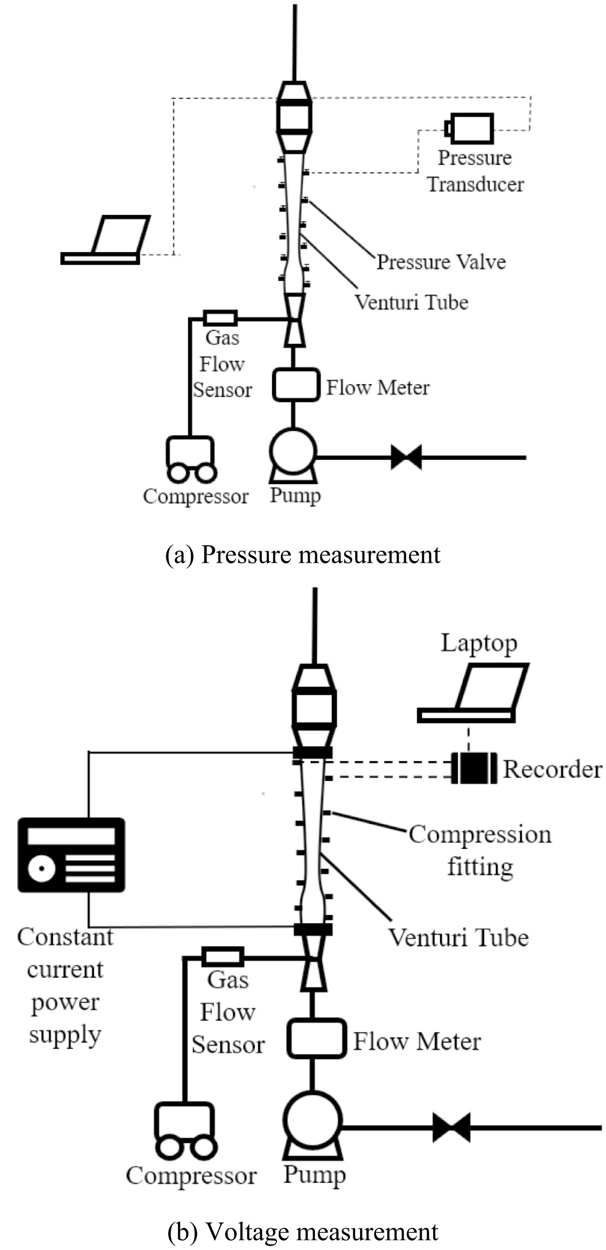

Fig. 7 Pressure measurement and voltage measurement setup

3 Result

3.1 Visualization result

To present a better understanding of the phenomenon inside the Venturi tube as the throat size was reduced, the flow visualization in single-phase flow conditions is presented in Fig. 8 for different j_{th}. As can be seen from the figure, in the range of the experiment condition, cavitation (highlighted in the dashed line box) was first clearly observed at lower velocity for smaller throat diameter, at $j_{th} = 20$ m/s for $d_{th} = 4$ mm, and at $j_{th} = 25$ m/s for $d_{th} = 6$ mm. Although the flow was under the same superficial throat velocity, the cavitation along the wall was prone to emerge earlier in the reduced throat diameter Venturi tube. As the velocity increased, the cavity length for $d_{th} = 4$ mm was longer than $d_{th} = 6$ mm with the cavity tail exceeding $z = 27$ mm. Next, while ensuring the throat velocity was maintained as the single-phase in Fig. 8, the flow was aerated with $\beta = 0.016$ of air to create an aerated flow condition and the result obtained is presented in Fig. 9.

In the aerated flow condition, bubbles were observed along the liquid flow whereas, in a single-phase flow, only liquid existed initially. For all tubes, it was observed that the

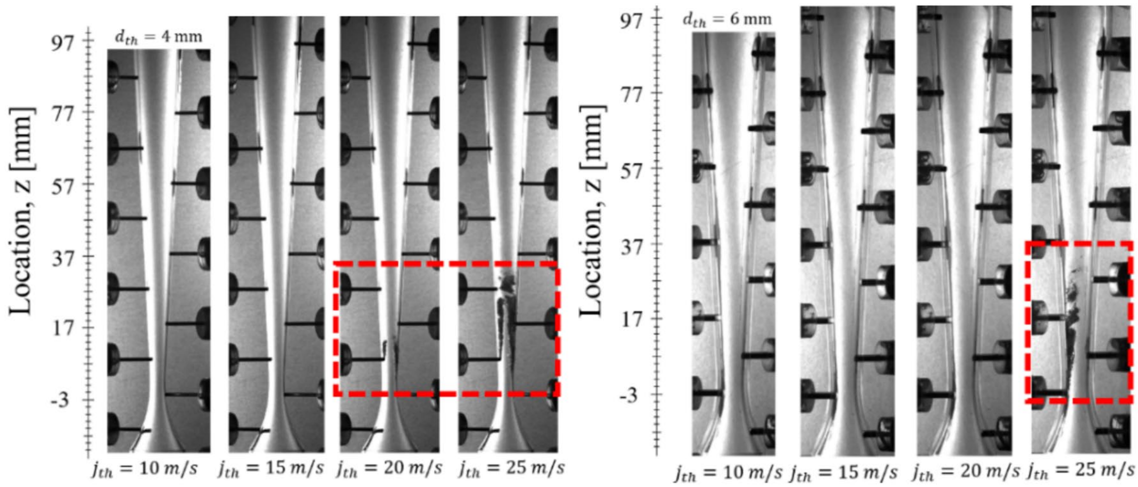

Fig. 8 Flow visualization of single-phase flow

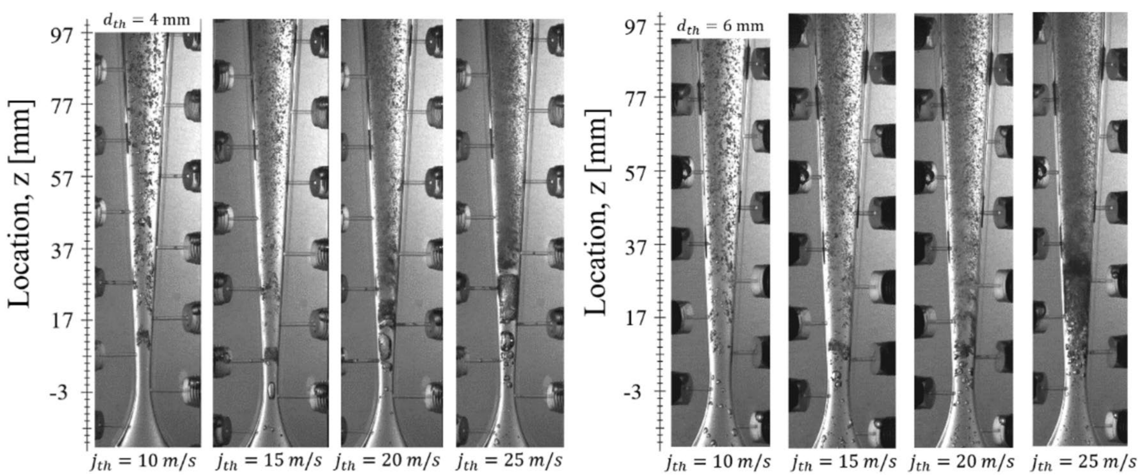

Fig. 9 Flow visualization of multiphase flow with $\beta = 0.016$

aeration went through the tube in the form of bubbles, and the bubbles collapsed after going through the throat area, with two different collapse mechanisms. Under the lower superficial throat velocity ($j_{th} = 10$ & 15 m/s for $d_{th} = 4$ mm, $j_{th} = 10$, 15 & 20 m/s for $d_{th} = 6$ mm), the bubbles sheared into smaller pieces due to slip velocity while in higher superficial throat velocity ($j_{th} = 20$ & 25 m/s for $d_{th} = 4$ mm, $j_{th} = 25$ m/s for $d_{th} = 6$ mm), the bubbles expanded before shrunk into smaller pieces.

This result has been reported by other similar studies on the bubble breakup mechanism which suggested that at the throat area, velocity was subsonic when tear-up happened and supersonic when expansion and shrinkage occurred (Fujiwara et al. 2007).

Interestingly, cavitation bubbles that emerged along the wall under the single-phase condition were not observed when aeration was performed. What stood out was, in high-velocity flow conditions, after the bubbles went through the throat area, a trailing streamer started to exist from the tail of the bubble. It was as if the bubble was ruptured from its initial shape, but it was not the case. As the bubble expanded in size, it lost its symmetry and wrinkles appeared on the surfaces of the bubbles. These wrinkles were observed to exist throughout the expanded volume of the bubbles. The close-up visualization of wrinkles observed during bubble expansion is shown in Fig. 10.

In Fig. 10, two conditions of high velocity for a $d_{th} = 4$ mm Venturi tube were chosen as the wrinkles were more obvious. In both cases, bubbles expanded after going through the throat area and as the expanded bubble traveled, wrinkles existed on the surface, before it collapsed and microbubbles were generated. The existence of wrinkles on the bubble surface was identical to other research related to bubble cavitation (where cavitation existed on bubbles).

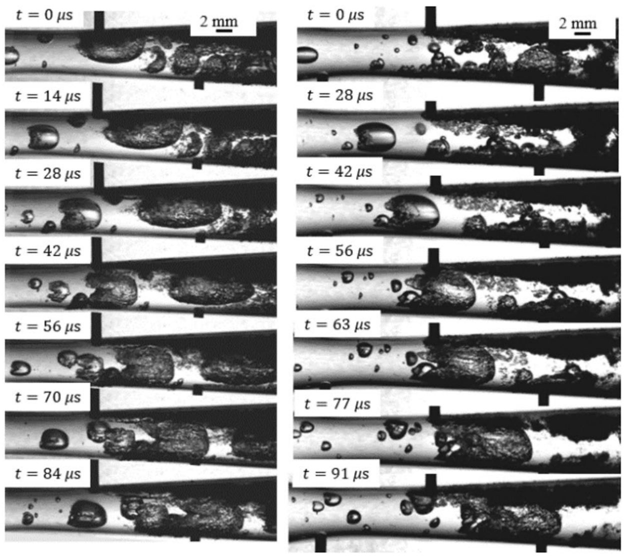

Fig. 10 Close-up visualization of wrinkles observed during bubble expansion in a $d_{th}=4$ mm tube at $j_{th}=25$ m/s

It was suggested that in the case of aerated flow condition, as a substitute for the cavitation along the tube's wall, the cavitation exists in the form of traveling bubble cavitation, before collapsing. This same theory was also proposed by De Chizelle et al. (1995) who labeled the wrinkles as surface instabilities that represent cavities' appearance (De Chizelle et al. 1995). However, in his illustration, surface instabilities were not represented, but the whole process was identical to our studies.

Therefore, in the later discussion of this investigation, this traveling bubble cavitation will be discussed concerning the pressure difference, velocity, and cavitation number. Although bubble cavitation was not observed in low-velocity flow conditions, the result will be presented too as a reference for discussion.

3.2 Pressure measurement and void fraction result

The next session of this investigation was concerned with further description of the flow behavior inside the different throat sizes of Venturi tubes, and the result of pressure measurement and calculated void fraction is presented in Fig. 11. From this point onward, only the results for aerated flow will be presented.

In general, for all cases, as the flow velocity increased, the inlet pressure was higher and the pressure drop was greater around the throat area before recovering. The pressure drop region also extended further downstream as velocity increased. At the same time, the void fraction peak also increased around the pressure drop region, as the velocity increased. It was also apparent that the different airflow ratios did not have a significant effect on pressure changes,

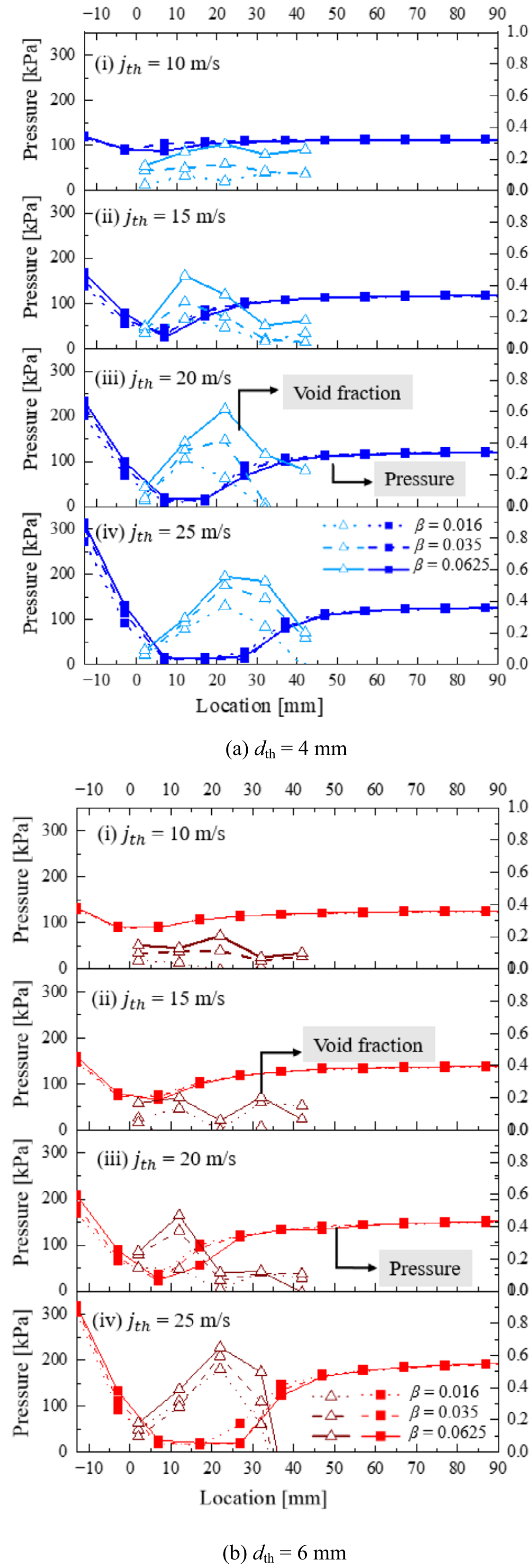

Fig. 11 Pressure and void fraction result

but an opposite trend was observed for the void fraction as increasing the airflow ratio increased the void fraction.

This pressure drop and void fraction trend were directly related to the bubble breakup characteristics in the Venturi tube. In low velocity, as the pressure dropped at the throat area due to space constrain, the velocity of the flow increased. It created slip velocity between the flowing liquid and bubble interface which caused the shearing and tearing up of bubbles into small pieces. In this condition, the void fraction in the Venturi tube had no dramatic changes as no bubble expansion occurred. Subsequently, as the velocity of the flow increased, the pressure dropped further lower at the throat area, and the void fraction increased too. Past research suggested that the peak in void fraction corresponded to the point of bubble expansion just before the bubble broke into microbubbles (Fujiwara et al. 2007).

As mentioned in visualization result, although the bubbles were observed as if the wall was ruptured, this expansion occurrence proves that the bubble wall was still intact. Therefore, it complies with the ideal gas law by expanding its volume when the surrounding pressure on the bubble decreases. As the volume expanded, the internal pressure of the bubbles was assumed to decrease too. Flowing downstream, the surrounding liquid regained bigger space to flow, and the surrounding pressure recovered. The sudden increase in pressure from the flowing liquid suppressed the bubble and ruptured the bubble's wall which caused it to disperse into small pieces known as microbubbles. Several studies discuss bubble fragmentation into microbubbles based on the velocity condition of the flow (Lee et al. 2019, 2021).

Interestingly, when comparing the void fraction for the two lower and the two higher throat velocities across different throat sizes, it was exhibited that for $d_{th} = 4$ mm, the peak around the throat area increased as the throat velocity increased. Unlikely for $d_{th} = 6$ mm, the void fraction peak for the two lower throat velocities exhibited insignificant differences. The observation was associated with the space in the throat area and the pressure drop scale. A smaller throat diameter resulted in a greater decrease in pressure, causing the bubble to expand larger than bubbles in a $d_{th} = 6$ mm throat diameter, even at the same throat velocity. As the velocity of the throat increased, both tubes showed a notable shift in the void fraction peak. Referring to Fig. 11 a)(iv) and b)(iv), the void fraction peak of both tubes was observed to be in the same range. This was due to the space constraint that inhibits the expansion of the bubble, especially for $d_{th} = 4$ mm.

3.3 Cavitation number

In order to further analyze the result associated with the cavitation phenomenon, a dimensionless number called cavitation number was utilized as presented in Eq. (4), where P_∞ stands for the pressure downstream near the outlet and P_v represents the saturated vapor pressure at T_∞, while ρ_l and U_z are the liquid density and the local velocity, respectively. The equation for the velocity was presented in Eq. (5). It was derived from the conservation of mass where the mass flow rate through a tube was assumed to be constant. Q_L was the liquid flow rate, α_z was the local void fraction retrieved from the void fraction measurement result, and A_z was the tube cross-sectional area. Figure 12 demonstrates the cavitation number changes throughout the Venturi tube where velocity calculation using void fraction result was applied. The cavitation number calculation point was at the throat area where $z = 2$ mm.

$$\sigma = \frac{P_\infty - P_V(T_\infty)}{\frac{1}{2}\rho_l U_z^2} \tag{4}$$

$$U_z = \frac{Q_L}{(1 - \alpha_z)A_z} \tag{5}$$

The interesting point to note in Fig. 12 was how the velocity scattered between the range of 10–30 m/s although the preliminary calculation for the experiment condition setup ranged between 10 and 25 m/s. As the calculation of the velocity in the graph considered void fraction result retrieved from measurement data, this suggested that the aerated air greatly affected the flowing fluid velocity. As seen in the graph, for both tubes, the cavitation number decreased along with the increase in velocity. The trend of reduction was also observed to be similar.

Next, Fig. 13 shows the result of different airflow ratios toward the cavitation number of the different throat-diameter

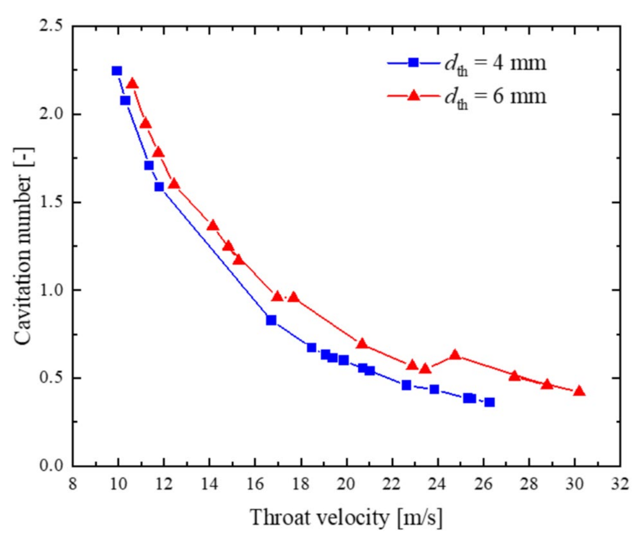

Fig. 12 Changes of cavitation with throat velocity calculated with consideration of void fraction inside the tube

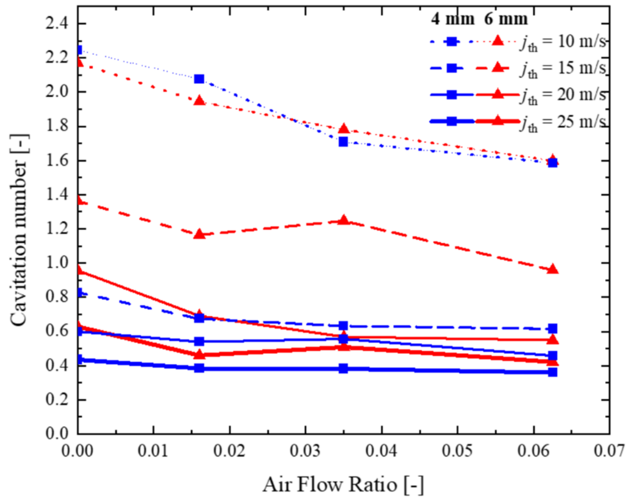

Fig. 13 Changes of cavitation number with airflow ratio for different throat velocity

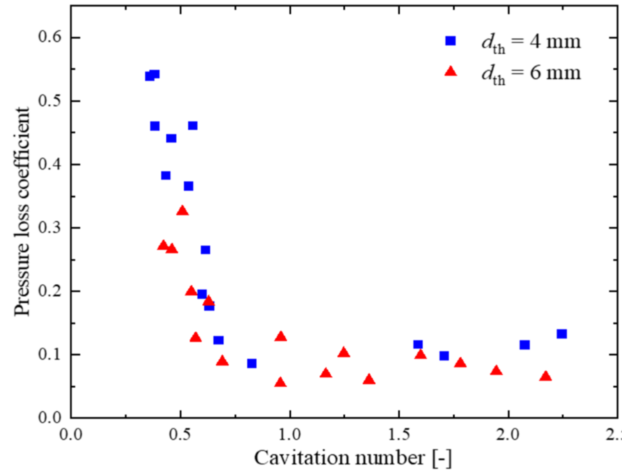

Fig. 14 Changes of cavitation number with pressure loss

Venturi tubes. In the non-cavitated single-phase flow (by referring to the visualization result of the single-phase in Fig. 8), increasing the airflow ratio decreased the cavitation number. The trend proposed that the injection of air into a non-cavitated flow, with a condition that the liquid flow rate was maintained constant, triggered the cavitation phenomenon The cavitation existed as a traveling cavitated bubble as shown in Fig. 10.

These cavitated bubbles on the surface of the main bubbles are believed to trigger the generation of smaller bubbles during the collapse of the bigger bubble. Brennen (2002) mentioned that in a bubbly cavitating flow, smaller size bubbles grow explosively when they go through a low-pressure environment and collapse as they flow out into a higher-pressure environment (Brennen 2002). As the main bubble collapse together with the cavitated bubble, the generation of smaller microbubbles could be achieved. In order to prove our theory, the relationship between the cavitation number and the generated bubble sizes will be discussed further in Microbubble distribution.

However in a cavitated single-phase flow (by referring to the visualization result of the single-phase in Fig. 8), especially a fully developed cavitated flow, an increase in airflow ratio did not contribute further drop to the cavitation number. It was suggested that in a fully developed single-phase cavitated flow, injection of air while maintaining the liquid flow rate has no significant effect on the cavitation phenomenon as the phenomenon has been fully developed.

Next, the pressure loss coefficient was calculated based on Eq. (6), and the result is presented in Fig. 14. As observed, when the cavitation decreased further after a certain cavitation number, the pressure loss started to increase significantly. The trend for both tubes was somehow similar, but the lower cavitation number cases for $d_{th} = 4$ mm outnumbered $d_{th} = 6$ mm. The explanation for this result was suggested by Fig. 12 where aeration affected the fluid velocity in the tube and higher fluid velocity caused greater pressure drop and contributed to a lower cavitation number. The lower cavitation number for $d_{th} = 4$ mm also suggested that aeration promoted the cavitation phenomenon earlier in the smaller throat-diameter Venturi tube.

$$L_C = \frac{P_{in} - P_{out}}{\frac{1}{2}\rho_L {v_{th}}^2} \quad (6)$$

3.4 Microbubbles distribution

As the main purpose of the Venturi tube was to generate microbubbles, the generated bubbles distribution was then analyzed in regard to the flow condition. Considering all flow conditions, the result of the generated bubbles is presented in Fig. 15. As can be observed from the graph, the bubble distribution results concentrated around the diameter of 0.2 mm and below.

To further investigate the relationship between cavitation number and generated microbubbles, the Sauter mean diameter (SMD) of generated microbubbles was calculated with Eq. (7), and the result is presented in Fig. 16. The SMD was calculated considering all bubbles identified through the image processing method mentioned in Sect. 2.2. Different throat velocities were represented with different symbols (indicated in the graph in black color), while the different airflow ratio was differentiated with different marks inside the symbols. The result for $j_{th} = 10$ m/s was not included in this result as cavitation was not prominent in the flow.

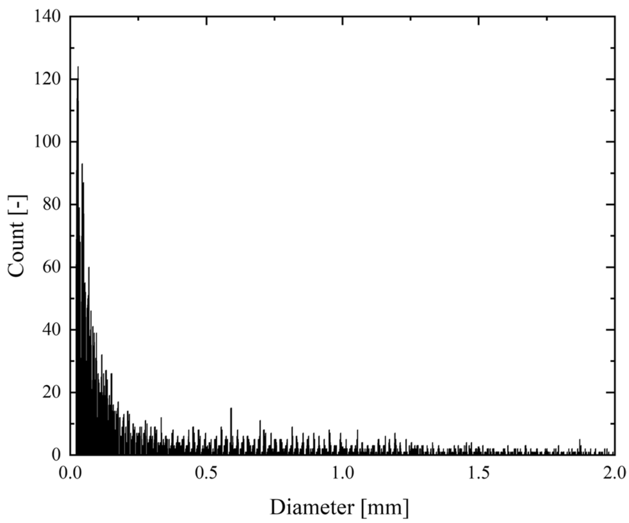

Fig. 15 Bubble distribution result for all cases

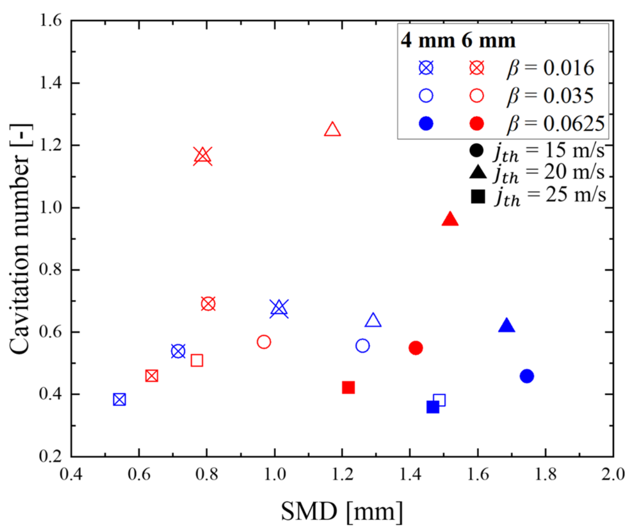

Fig. 16 Cavitation number changes with SMD

$$d_{32} = \frac{\sum d_{out}^{3}}{\sum d_{out}^{2}} \quad (7)$$

As mentioned in Sect. 3.3, the cavitation number decreased with the increase in velocity. Increasing the airflow ratio under the same flow velocity intensified the cavitation occurrence. Nonetheless, referring to Fig. 16, although the cavitation number at the throat tends to become smaller with a higher airflow ratio for almost all conditions, the SMD result demonstrated a contradicting trend. As the airflow ratio for each flow increased, the bubbles SMD were bigger regardless of the cavitation number. Observing the result in terms of different throat diameters provides a different perspective. For the two highest velocities, the SMD was smaller for $d_{th} = 4$ mm at the lowest airflow ratio, but the trend turned over when the airflow ratio increased.

Next, the probability density function (PDF) of generated microbubbles for a diameter of less than 0.2 mm, under different flow conditions, is presented in Fig. 17. Bubbles less than 0.2 mm were given focus in this result to evaluate the generation of microbubbles under each different flow condition.

In general, the PDF for $d_{th} = 4$ mm was higher than $d_{th} = 6$ mm for all flow conditions. The bubble diameter frequency has a higher concentration at a smaller diameter for all conditions. Both tubes displayed a similar trend where increasing the fluid velocity resulted in a lower PDF of smaller bubbles for the highest airflow ratio, but the trend was more obvious for $d_{th} = 6$ mm. Observing the graph under each different throat velocity revealed that under low throat velocity of (i) $j_{th} = 10$ m/s, the PDF increased with airflow ratio for both tubes. Nevertheless, the trend was different at a throat velocity of (ii) $j_{th} = 15$ m/s. Referring to Fig. 17 (a)(ii), the PDF was slightly higher at a smaller diameter for the highest airflow ratio but was at the same level for the other two lower airflow ratios. In contrast, Fig. 17 (b)(ii) illustrates that the PDF for two higher airflow ratios was at the same level, while the lowest airflow ratio resulted in a lower PDF of smaller bubbles. $d_{th} = 6$ mm exhibited the same trend for the flow condition of (iii) $j_{th} = 20$ m/s and (iv) $j_{th} = 25$ m/s, whereas the trend for $d_{th} = 4$ mm slightly changed at (iv) $j_{th} = 25$ m/s. Although the relationship between the generated microbubbles with flow conditions did not seem to be straightforward, we believe that cavitation plays an important role in the production of smaller microbubbles as reduced throat diameter produced a higher PDF of microbubbles.

These findings suggested that the tendency of bubble distributions for less than 0.2 mm microbubbles and the tendency for SMD were different for aerated Venturi tubes. Reducing the throat diameter promoted the production of smaller bubbles, where higher velocity of fluid with minimum airflow ratio is favorable.

This occurs because a Venturi tube with a smaller throat diameter creates a higher-pressure difference between the outlet and the throat, leading to greater pressure loss. As shown in Fig. 14, cavitation became more effective as the pressure loss increased significantly. This loss transforms into high-pressure pulsations, which then impacts nearby bubbles, resulting in the formation of more, smaller bubbles in a smaller throat Venturi tube. This discovery will assist researchers in tailoring bubble generation, whether based on average size or distribution.

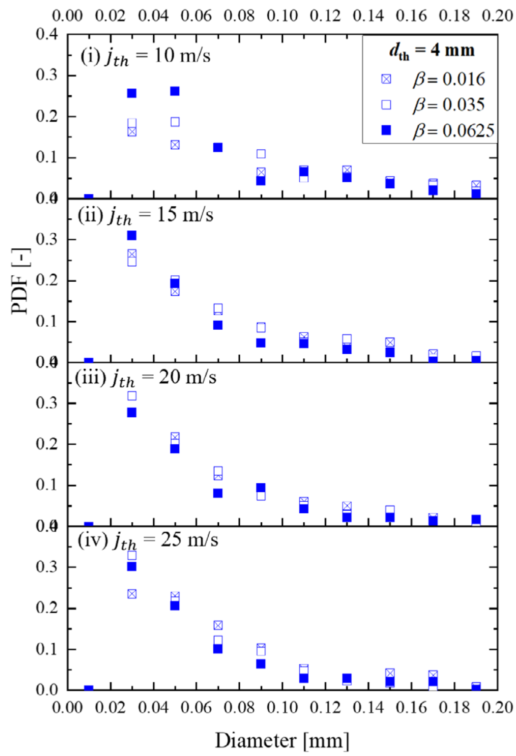

(a) d_{th} = 4 mm

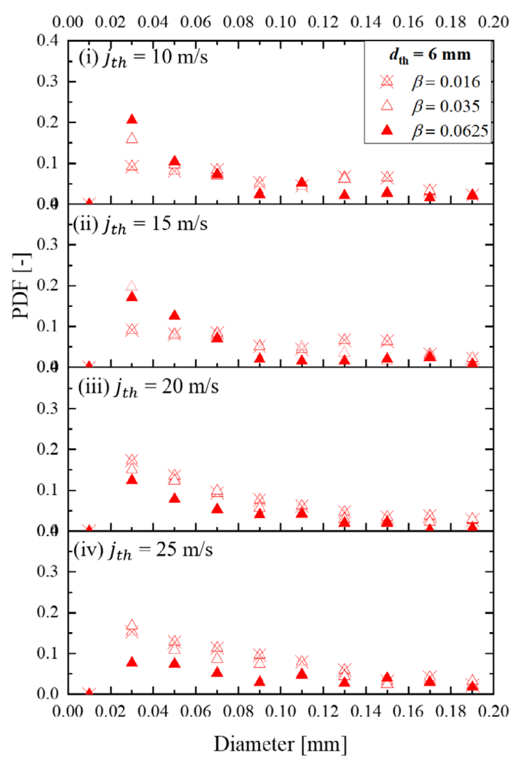

(b) d_{th} = 6 mm

Fig. 17 PDF of generated microbubbles

4 Conclusion

In this investigation, the aim was to investigate the cavitation number changes in aerated Venturi tube as we reduced the throat diameter and the effects of cavitation number on the generated microbubbles. Visualization of flow, the result for pressure, and void fraction along the tube of both different throat sizes were compared and analyzed. The microbubbles produced especially below 0.2 mm in diameter by both tubes were also evaluated. The following conclusion was suggested.

1. The visualization result revealed that in present experiment range, reducing the throat diameter triggered the occurrence of the cavitation phenomenon earlier even at the same throat velocity.
2. Aeration done in this experiment decreased the cavitation number significantly for a non-cavitated single-phase flow but did not contribute much to a fully developed cavitated single-phase flow.
3. In an aerated flow condition for both tubes, cavitation existed as traveling bubble cavitation. Increasing the velocity of the flow caused the traveling bubble to expand, and cavity existed as instabilities on the bubble's surface. In the present study, reducing the throat size Venturi tube resulted in higher PDF of bubbles less than 0.2 mm in diameter either for cavitated flow conditions or non-cavitated flow conditions.
4. The result of the cavitation number effects on the SMD was not prominent in this study compared to the effect of flow velocity on the SMD. Higher velocity produces smaller bubbles, while a higher airflow ratio increases the sizes of the bubbles, on average.

Acknowledgements The author would like to thank Mr. Fujiwara Kouta and Saito Shinpei for their help in reviewing this paper before submission. This paper was published with the sponsor from the Young Researcher Training Program grant from the University of Tsukuba.

Author contribution N.S.H wrote the main manuscript text and data analysis. A.K. contributed to the experiment design and revising the manuscript critically. All authors reviewed the manuscript and involved in the discussion to finalize the manuscript.

Data availability No datasets were generated or analyzed during the current study.

Declarations

Conflict of interest The authors declare no competing interests.

References

Bashir TA, Soni AG, Mahulkar AV, Pandit AB (2011) The CFD driven optimisation of a modified venturi for cavitational activity. Can J Chem Eng 89:1366–1375. https://doi.org/10.1002/cjce.20500

Brennen CE (2002) Fission of collapsing cavitation bubbles. J Fluid Mech 472:153–166. https://doi.org/10.1017/S0022112002002288

De Chizelle YK, Ceccio SL, Brennen CE (1995) Observations and scaling of travelling bubble cavitation. J Fluid Mech 293:99–126. https://doi.org/10.1017/S0022112095001650

Fujii K, Kaneko A, Abe Y & Ike M (2018) Bubble collapse behavior and pressure wave propagation due to bubble miniaturization in a Venturi tube. In: proceeding of the 23rd national symposium on power and energy system, 14–15 June 2018. https://doi.org/10.1299/jsmepes.2018.23.C141

Fujiwara A, Okamoto K, Hashiguchi K, Peixinho J, Takagi S & Matsumoto Y (2007) Bubble breakup phenomena in a Venturi tube. In: proceedings of the ASME/JSME 2007 5th Joint Fluids Engineering Conference, Vol. 1: Symposia, Parts A and B, San Diego, California, USA, July 30–August 2, 2007, pp. 553–560. ASME. https://doi.org/10.1115/FEDSM2007-37243

Gordiychuk A, Svanera M, Benini S, Poesio P (2016) Size distribution and Sauter mean diameter of micro bubbles for a Venturi type bubble generator. Exp Therm Fluid Sci 70:51–60. https://doi.org/10.1016/j.expthermflusci.2015.08.014

Huang J, Sun L, Mo Z et al (2019) A visualized study of bubble breakup in small rectangular Venturi channels. Exp Comput Multiph Flow 1:177–185. https://doi.org/10.1007/s42757-019-0018-x

Huang J, Sun L, Mo Z et al (2021) Experimental investigation on the effect of throat size on bubble transportation and breakup in small Venturi channels. Int J of Multiphase Flow. https://doi.org/10.1016/j.ijmultiphaseflow.2021.103737

Kido N, Kaneko A, Abe Y, Ike M (2021) Bubble collapse phenomenon of multiphase flow field in a Venturi tube. Jpn J Multiphase Flow 35:51–59. https://doi.org/10.3811/jjmf.2021.009

Lee CH, Choi H, Jerng DW et al (2019) Experimental investigation of microbubble generation in the venturi nozzle. Int J Heat Mass Transf 136:1127–1138. https://doi.org/10.1016/j.ijheatmasstransfer.2019.03.040

Lee CH, Wongwises S, Jerng DW, Ahn HS (2021) Experimental study on breakup mechanism of microbubble in 2D channel. Case Studies Thermal Eng 28:101523. https://doi.org/10.1016/j.csite.2021.101523

Li M, Bussonnière A, Bronson M et al (2019) Study of Venturi tube geometry on the hydrodynamic cavitation for the generation of microbubbles. Miner Eng 132:268–274. https://doi.org/10.1016/j.mineng.2018.11.001

Liu Y, Fan H, Wu D et al (2020) Experimental investigation of the dynamic cavitation behavior and wall static pressure characteristics through convergence-divergence venturis with various divergence angles. Sci Rep 10:14172. https://doi.org/10.1038/s41598-020-68317-3

Ni R (2024) Deformation and breakup of bubbles and drops in turbulence. Annu Rev Fluid Mech 56:319–347. https://doi.org/10.1146/annurev-fluid-121021

Saffreena N and Kaneko A (2022) Cavitation effects on bubble breakup characteristics in a Venturi tube. In: 7th Thermal and Fluids Engineering Conference (TFEC) Las Vegas, 15–18 May 2022, ASTFE Digital, p 1195–1203. ASTFE Digital Library. https://doi.org/10.1615/TFEC2022.ref.040773

Sun L, Mo Z, Zhao L et al (2017) Characteristics and mechanism of bubble breakup in a bubble generator developed for a small TMSR. Ann Nucl Energy 109:69–81. https://doi.org/10.1016/j.anucene.2017.05.015

Terasaka K, Hirabayashi A, Nishino T et al (2011) Development of microbubble aerator for waste water treatment using aerobic activated sludge. Chem Eng Sci 66:3172–3179. https://doi.org/10.1016/j.ces.2011.02.043

Tomov P, Khelladi S, Ravelet F et al (2016) Experimental study of aerated cavitation in a horizontal venturi nozzle. Exp Therm Fluid Sci 70:85–95. https://doi.org/10.1016/j.expthermflusci.2015.08.018

Uesawa SI, Kaneko A, Abe Y (2012) Measurement of void fraction in dispersed bubbly flow containing micro-bubbles with the constant electric current method. Flow Measur Instrum 24:50–62. https://doi.org/10.1016/j.flowmeasinst.2012.03.010

Wen LH, Bin IA, Menon PM et al (2011) Case studies of microbubbles in wastewater treatment. Desalination Water Treat 30:10–16. https://doi.org/10.5004/dwt.2011.1217

Wijngaarden LV (1972) One-dimensional flow of liquids containing small gas bubbles. Annu Rev Fluid Mech 4:369–396. https://doi.org/10.1146/annurev.fl.04.010172.002101

Zhao L, Mo Z, Sun L et al (2017) A visualized study of the motion of individual bubbles in a venturi-type bubble generator. Prog Nucl Energy 97:74–89. https://doi.org/10.1016/j.pnucene.2017.01.004